IOPscience iopscience.iop.org

Home Search Collections Journals About Contact us My IOPscience

The singular approach for processing polarization-inhomogeneous laser images of blood plasma layers

This article has been downloaded from IOPscience. Please scroll down to see the full text article.

2013 J. Opt. 15 044030

(http://iopscience.iop.org/2040-8986/15/4/044030)

View the table of contents for this issue, or go to the journal homepage for more

Download details:
IP Address: 92.112.188.169
The article was downloaded on 09/06/2013 at 14:18

Please note that terms and conditions apply.

IOP Publishing Journal of Optics
J. Opt. **15** (2013) 044030 (8pp) doi:10.1088/2040-8978/15/4/044030

The singular approach for processing polarization-inhomogeneous laser images of blood plasma layers

P O Angelsky[1], A G Ushenko[1], A V Dubolazov[1], M I Sidor[1], G B Bodnar[2], G Koval[2] and L Trifonyuk[3]

[1] Optics and Spectroscopy Department, Chernivtsi National University, 2 Kotsyubinsky Street, Chernivtsi 58012, Ukraine
[2] Bukovinian State Medical University, 3 Theater Square, Chernivtsi, Ukraine
[3] Rivne Regional Oncological Hospital, 12 Olesya Street, Rivne, 33001, Ukraine 58000, Ukraine

E-mail: yuriyu@gmail.com

Received 2 November 2012, accepted for publication 5 February 2013
Published 10 April 2013
Online at stacks.iop.org/JOpt/15/044030

Abstract
We present in this work the results of an investigation to analyse the coordinate distributions of azimuths and ellipticity of polarization (polarization maps) in laser images of blood plasma layers for three groups of patients: healthy (group 1), mastopathy (group 2) and breast cancer (group 3). To characterize polarization maps for all groups of samples we use three groups of parameters: statistical moments of the first to fourth orders, autocorrelation functions and logarithmic dependences for power spectra related to distributions of azimuths and ellipticity of polarization inherent to laser images of blood plasma. We ascertain the criteria for diagnosis and differentiation of pathological changes of the breast.

Keywords: polarization, birefringence, statistical optics, medical and biological imaging

1. Introduction

Traditionally, the processes of transforming optical radiation of phase-inhomogeneous objects and media have been considered using statistical approaches (e.g. the theory of radiation transfer by Monte Carlo modeling [1, 2]).

The most common traditional methods for studying the scattering of light fields can be separated into the following independent categories: 'scalar' (photometry and spectrophotometry) [3, 4] and 'vector' (polarization nephelometry, Mueller-matrix optics) [5–9].

Using these approaches, we can determine the interrelations between the sets of statistical moments of the 1st to 4th orders, correlation functions, fractal dimensionalities [10–18] that characterize phase-inhomogeneous biological layers, and coordinate distributions for phases, azimuths and ellipticity of polarization in their laser images.

A new step in the investigation of vector field structure is the singular approach [19, 20]. The main feature of this approach is the analysis of definite polarization states to determine the whole structure of coordinate distributions for azimuths and ellipticities of polarization. The so-called polarization singularities are commonly used as these states:

- states with linear polarization when the direction of rotation of the electric field vector is indefinite, the so-called *L*-states;
- circularly polarized states when the azimuth of polarization of the electric field vector is indefinite, the so-called *C*-states.

Investigations of the coordinate distributions of such discrete states in the field of scattered radiation allow its topographic polarization structure to be restored. Such an approach has becomes the subject of numerous investigations forming the new approach of singular optics [21–34].

At the same time, the majority of works on singular optics have a theoretical character, taking into account interference–diffraction mechanisms of the formation of the polarization-singular structure of coherent fields. Meanwhile,

 © 2013 IOP Publishing Ltd Printed in the UK & the USA

the process of formation of networks of polarization singularities in the images of optically anisotropic objects is insufficiently investigated. Therefore, the fundamental task of investigating the interconnection between the anisotropy parameters of such objects and the networks of polarization singularities of their images is topical. In addition, the applied aspect—using the discrete selection of polarization states of images of a biological layer to diagnose changes due to disease states from changes in anisotropy parameters—is important. A promising object in this regard is blood plasma: this biological fluid is easily accessible and it polycrystalline structure carries information about a number of pathological states [35, 36].

This work is aimed at ascertaining the possibilities of diagnosing and classifying pathological changes of the breast by means of determining the values and ranges for changes in the statistical (moments of the first to fourth orders), correlation (autocorrelation functions) and fractal (logarithmic dependences for power spectra) parameters that characterize coordinate distributions for polarization-singular states in laser images of blood plasma layers.

2. Polarization modeling of properties inherent to networks of biological protein crystals in blood plasma layers

As the object of investigation we have used optically thin (geometric thickness $l \approx 15$–20 μm, attenuation coefficient $\tau < 0.1$) blood plasma smears dried at room temperature. Such a choice of sample is traditional in medical laboratory diagnostics. From the optical point of view, such samples are single scattered. This fact allows us to minimize the influence of speckle background in laser images.

As a basis for analysis of the processes forming polarization-inhomogeneous images of a blood plasma layer, we use the optical model developed in [37]:

- Optical properties of the blood plasma layer are determined as those of a two-component amorphous-crystalline structure.
- The amorphous component attenuates the intensity of the illuminating laser beam, while the polarization state remains the same.
- The crystalline component is an architectural net consisting of uniaxial birefringent amino-acid crystals and can be described by the Mueller matrix [38]:

$$W = \left\| \begin{matrix} 1 & 0 & 0 & 0 \\ 0 & w_{22} & w_{23} & w_{24} \\ 0 & w_{32} & w_{33} & w_{34} \\ 0 & w_{42} & w_{43} & w_{44} \end{matrix} \right\| = \left\| \begin{matrix} 1 & 0 & 0 & 0 \\ 0 & \cos^2 2\rho + \sin^2 2\rho \cos\delta & \cos 2\rho \sin 2\rho (1 - \cos\delta) & -\sin 2\rho \sin\delta \\ 0 & \cos 2\rho \sin 2\rho (1 - \cos\delta) & \sin^2 2\rho + \cos^2 2\rho \cos\delta & \cos 2\rho \sin\delta \\ 0 & \sin 2\rho \sin\delta & -\cos 2\rho \sin\delta & \cos\delta \end{matrix} \right\|. \quad (1)$$

Here ρ is the direction (orientation azimuth) of the fast axis; $\delta = 2\pi/\lambda \Delta n l$ the value of the phase shift between orthogonally linearly polarized components of laser amplitude at a point with coordinates $r \equiv (x, y)$; λ is the wavelength; l the geometric path; and $\Delta n \approx 1.2 \times 10^{-2}$ the index of birefringence.

- The polarization transformation processes for an optically uniaxial crystal at a point with coordinates $r \equiv (x, y)$ can be described using the following vector-parametric equation:

$$S^*(r) = \{W\} S_0, \quad (2)$$

where S_0, S^* are the Stokes vectors of objects illuminated and transformed by the beam, respectively.

Using the matrix equation (2) with operator structure (1) and a linear state of the probing laser beam polarization ($S^0 = \begin{pmatrix} 1 \\ \cos 2\alpha_0 \\ \sin 2\alpha_0 \\ 0 \end{pmatrix}$), where α_0 is the azimuth, it is possible to determine the primary polarization structure (azimuth-alpha and ellipticity-beta) at points of the blood plasma layer image

$$\alpha(r) = 0.5 \arctan \left(\frac{w_{32} \cos 2\alpha_0 + w_{33} \sin 2\alpha_0}{w_{22} \cos 2\alpha_0 + w_{23} \sin 2\alpha_0} \right), \quad (3)$$

$$\beta(r) = 0.5 \arcsin(\sin\delta \sin 2(\rho - \alpha_0)), \quad (4)$$

where $w_{ik}(\rho, \delta)$ are the elements of matrix (1).

Following from the analytical relations (3) and (4) among the whole set of values $(\alpha(r); \beta(r))$, formation of L and $\pm C$ polarization states seems to be very probable

$$\beta(r) = 0 \Rightarrow ''L-'' \Leftrightarrow \delta(r) = q\pi, \qquad q = 0; 1; 2; \ldots \quad (5)$$

$$\beta(r) = \pm 0.25\pi \Rightarrow \pm C- \Leftrightarrow \delta(r) = (2q + 1)(0.5\pi). \quad (6)$$

In this work, to describe coordinate distributions for polarization-singular $(L, \pm C)$ states in laser images of blood plasma layers we have used the following characteristic values of the fourth Stokes vector (V_4) parameter in the corresponding points $r \equiv (x, y)$:

$$\begin{aligned} V_4(x, y) = 0 &\leftrightarrow L(\beta = 0); \\ V_4(x, y) = \pm 1 &\leftrightarrow \pm C(\beta = \pm 0.25\pi). \end{aligned} \quad (7)$$

3. Experimental setup for polarimetric investigations

Our study of polarization-inhomogeneous laser images of blood plasma layers was performed using the optical scheme of a laser polarimeter (see figure 1) [17, 39].

Illumination was performed using a parallel beam with cross-section $\varnothing = 10^4$ μm from a He–Ne laser ($\lambda = 0.6328$ μm) 1. The polarization illuminator (quarter-wave plates 3 and 5 as well as polarizer 4 (P)) were used to form various polarization states in the laser beam. Polarization images of laser images of blood plasma layers (6) were projected using the micro-objective (7; focal distance 30 mm, aperture 0.1, magnification 4×) into the plane of the light-sensitive area ($m \times n = 800$pixel $\times$ 600 pixel) in the CCD camera [10; The Imaging Source DMK 41AU02.AS, monochrome 1/2″ CCD, Sony ICX205AL (progressive scan); resolution 1280 × 960; size of light-sensitive area 7600 × 6200 μm; sensitivity 0.05 lx; dynamic range 8 bit; signal to

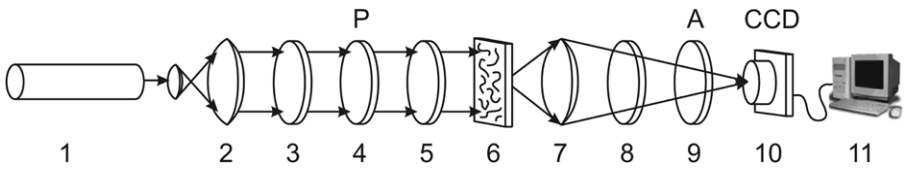

Figure 1. Optical scheme of the polarimeter: 1, He–Ne laser; 2, collimator; 3, 5, 8, quarter-wave plates; 4, 9, polarizer (P) and analyzer (A), respectively; 6, object under investigation; 7, micro-objective; 10, CCD camera; 11, personal computer.

noise ratio 9 bit; deviation of photosensitive characteristics from linear no more then 15%]. Turning the transmission axis of the analyzer (A) (9) by angles ±45° relative to the direction of the fast axis for the quarter-wave plate (8), we could determine the intensities of the right ($I_{\otimes}$) and left ($I_{\oplus}$) circularly polarized components for each separated pixel of the CCD camera (10). This served as a basis for calculating the coordinate distributions of the fourth parameter in the Stokes vector $V_4(r_{mn})$ describing the laser images of blood plasma layers, if using the relation

$$V_4(r_{mn}) = \frac{I_{\otimes}(r_{mn}) - I_{\oplus}(r_{mn})}{I_{\otimes}(r_{mn}) + I_{\oplus}(r_{mn})}. \tag{8}$$

The two-dimensional array (8) was scanned along the horizontal direction $x \equiv 1, \ldots, m$ with the step $\Delta x = 1$ pixel. For each horizontal line of array $V_4(r_{mn})$ we calculated the number ($N(x)$) of characteristic values $V_4 = 0$ and ±1.

Thus, we determined the dependences $N^i_L(x)$ and $N^i_{\pm C}(x)$ for amounts of polarization-singular $L-$ and $\pm C-$ points within the limits of a laser image of blood plasma layers. Here i is the number of horizontal lines ($i = 1, \ldots, n$).

4. Criteria for estimating polarization-inhomogeneous laser images of blood plasma layers

Distributions $N_{L;\pm C}(x)$ for the number of polarization-singular states in laser images of blood plasma layers are characterized by the set of statistical moments of the first to fourth orders $Z_{j=1;2;3;4}$ calculated using the following relations:

$$\begin{aligned} Z_1 &= \frac{1}{M}\sum_{i=1}^{M} |N^{(i)}_{L,\pm C}(x)|, \\ Z_2 &= \sqrt{\frac{1}{M}\sum_{i=1}^{M}[N^{(i)}_{L,\pm C}(x) - Z_1]^2}, \\ Z_3 &= \frac{1}{Z_2^3}\frac{1}{M}\sum_{i=1}^{M}[N^{(i)}_{L,\pm C}(x)]^2, \\ Z_4 &= \frac{1}{Z_2^4}\frac{1}{M}\sum_{i=1}^{M}[N^{(i)}_{L,\pm C}(x)]^4, \end{aligned} \tag{9}$$

where $M = 800 \times 600$ is the number of pixels in the CCD camera (10 in figure 1).

Our analysis of the coordinate structure for $N_{L;\pm C}(x)$ distributions was based on the autocorrelation method using the function [5]

$$K_{L;\pm C}(\Delta x) = \lim_{m\to 0}\frac{1}{m}\int_1^m N_{L;\pm C}(x) \times N_{L;\pm C}(x - \Delta x)\,\mathrm{d}x. \tag{10}$$

Here, ($\Delta x = 1$ pixel) is the step for changing the coordinate $x = 1$–m.

As correlation parameters that characterize the dependences $K_{L;\pm C}(\Delta x)$, we chose:

- the correlation area $S_{L;\pm C}$

$$S_{L;\pm C} = \int_1^m K_{L;\pm C}(\Delta x)\mathrm{d}x; \tag{11}$$

- the correlation moment $Q_{L;\pm c}$ that defines the excess for the distribution of values $K_{L;\pm C}(\Delta x)$

$$Q_{L;\pm C} = \frac{\sum_{i=1}^{m}(K_{L;\pm C}(\Delta x_i))^4}{\sum_{i=1}^{m}(K_{L;\pm C}(\Delta x_i))^2}. \tag{12}$$

Fractal analysis of the distributions $N_{L;\pm C}(x)$ was performed using the calculation of logarithmic dependences $\log J[N_{L;\pm C}(x)] - \log d^{-1}$ for the power spectra $J[N_{L;\pm C}(x)]$

$$J = \int_{-\infty}^{+\infty} N_{L;\pm C}\cos 2\pi\nu\,\mathrm{d}\nu, \tag{13}$$

where $\nu = d^{-1}$ are the spatial frequencies that are determined by the geometrical sizes (d) of laser images of structural elements in the blood plasma layers.

The dependences $\log J[N_{L;\pm C}(x)] - \log d^{-1}$ are approximated using the least-squares method into the curves $\Phi(\eta)$, straight parts of which serve to determine the slope angles η and calculate fractal F dimensionalities by using the relations [17]

$$F_{L;\pm C} = 3 - tg\eta. \tag{14}$$

Classification of coordinate distributions $N_{L;\pm C}(x)$ should be performed using the following criteria:

- they are fractal on the condition of a constant value of the slope angle $\eta = \text{const}$ for two to three decades of changing sizes d;
- they are multifractal, if several slope angles $\Phi(\eta)$ are available;
- they are random when any stable slope angles are absent within the whole range of changing sizes d.

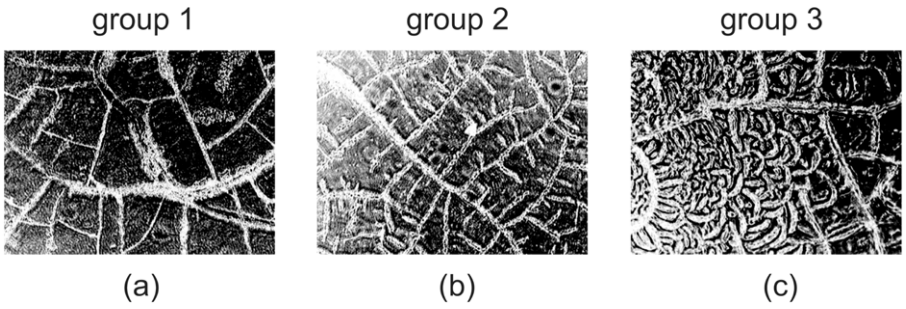

Figure 2. Coordinate distributions $V_4(m \times n)$ of laser images inherent to laser images of blood plasma layers.

In the latter case, the distributions $\log J[N_{L;\pm C}(x)] - \log d^{-1}$ are characterized by the dispersion

$$D_z = \sqrt{\frac{1}{m}\sum_{i=1}^{m}[\log J(N_{L;\pm C}(x_i)) - \log d^{-1}]^2}. \qquad (15)$$

5. Characterization of objects under investigation

Figure 2 illustrates coordinate (50 pixel × 50 pixel) distributions of the fourth parameter for the Stokes vector $V_4(m \times n)$ inherent to laser images of blood plasma layers in all the groups.

Our qualitative analysis of coordinate distributions $V_4(m \times n)$ for laser images of blood plasma layers (figure 2) enabled us to reveal:

- images of a healthy human blood plasma smear (figure 2(a)) consist of elliptically polarized regions of a polycrystalline network ($V_4(m \times n) \neq 0$) of protein crystals on a linearly polarized background ($V_4(m \times n) = 0$);
- the polarization-inhomogeneous component (figure 2(b)) is increased in the laser images of blood plasma layers from patients affected by mastopathy formed both by linearly ($V_4(m \times n) = 0$) and elliptically ($V_4(m \times n) \neq 0$) polarized states, including the circularly ($V_4(m \times n) = 1$) polarized one;
- the laser images of blood plasma layers of patients affected by breast cancer are characterized by the widest range of change the azimuth and ellipticity of polarization, which is connected with developed polycrystalline network (figure 2(c)) of albumin and globulin amino acids ($-1 \leq V_4(m \times n) \leq 1$).

6. Statistical, correlation and fractal analyses for distributions of polarization-singular states in laser images of blood plasma layers

6.1. L-states of laser images

Summarized in figure 3 is a series of coordinate ($V_4(m \times n) = 0$, fragments (a)–(c)), quantitative ($N_L(x)$, fragments (d)–(f)), autocorrelation ($K_L(\Delta m)$, fragments (g)–(h)) and logarithmic ($\log J_L - \log d^{-1}$, fragments (m)–(o)) distributions for polarization-singular L states in blood plasma layers laser images from all groups.

Our comparative analysis of the obtained dependences $N_L(x)$ for the number of polarization-singular L-states in laser images of blood plasma layers for all the groups (figures 3(d)–(o)) revealed a similarity in their statistical, correlation and fractal structures. For instance, all the $N_L(x)$ distributions are close to the equiprobable ones—the condition $Z^L_{j=3;4} \ll Z^L_{j=1;2}$ is valid for the values of statistical moments. Distinctions between the distributions of L-states in laser images of various blood plasma layers are observed as variations of the first and second statistical moments: $Z^L_1 = 0.59$; $Z^L_2 = 0.15$; $Z^L_3 = 0.06$; $Z^L_4 = 0.08$ (group 1); $Z^L_1 = 0.44$; $Z^L_2 = 0.22$; $Z^L_3 = 0.08$; $Z^L_4 = 0.088$ (group 2) and $Z^L_1 = 0.29$; $Z^L_2 = 0.36$; $Z^L_3 = 0.05$; $Z^L_4 = 0.06$ (group 3).

As seen, for laser images of blood plasma layers from the first, second and third groups, the mean value Z^L_1 is decreased 1.5 and 2.1 times. And vice versa, the dispersion Z^L_2 is increased 1.5 and 2.45 times. These changes in $N_L(x)$ distributions are related to the mechanisms of increasing of optical anisotropy (formation of elliptically polarized states in laser images) due to increases in concentration of blood plasma proteins.

The investigated statistical structure of L-states for polarization of laser images of blood plasma layers is confirmed by a monotonous drop of dependences for autocorrelation $K_L(\Delta m)$ functions of all the distributions $N_L(x)$ (figures 3(g), (l), (h)). In this case, values of the correlation area S and correlation moment Q trend to their boundary values $S^L \to 0.33$, $Q^L \to 0$, that are jsut characteristic of equiprobable distributions: $S^L = 0.24$, $Q^L = 0.12$ (group 1); $S^L = 0.22$, $Q^L = 0.14$ (group 2); $S^L = 0.18$, $Q^L = 0.19$ (group 3).

The performed analysis of logarithmic dependences $\log J_L - \log d^{-1}$ (figures 3(m)–(o)) for the power spectra $J(N_L)$ of the distribution $N_L(x)$ of laser images of blood plasma for all groups revealed a common regularity—the approximating curves are characterized by stable slope angles that corresponded to increases in the value of fractal dimensionalities: $F^L = 2.07$ (group 1), $F^L = 2.12$ (group 2) and $F^L = 2.15$ (group 3).

6.2. ±C states of laser images

Summarized in figure 4 is the series of coordinate ($V_4(m \times n) = 1$), quantitative ($N_{\pm C}(x)$), autocorrelation

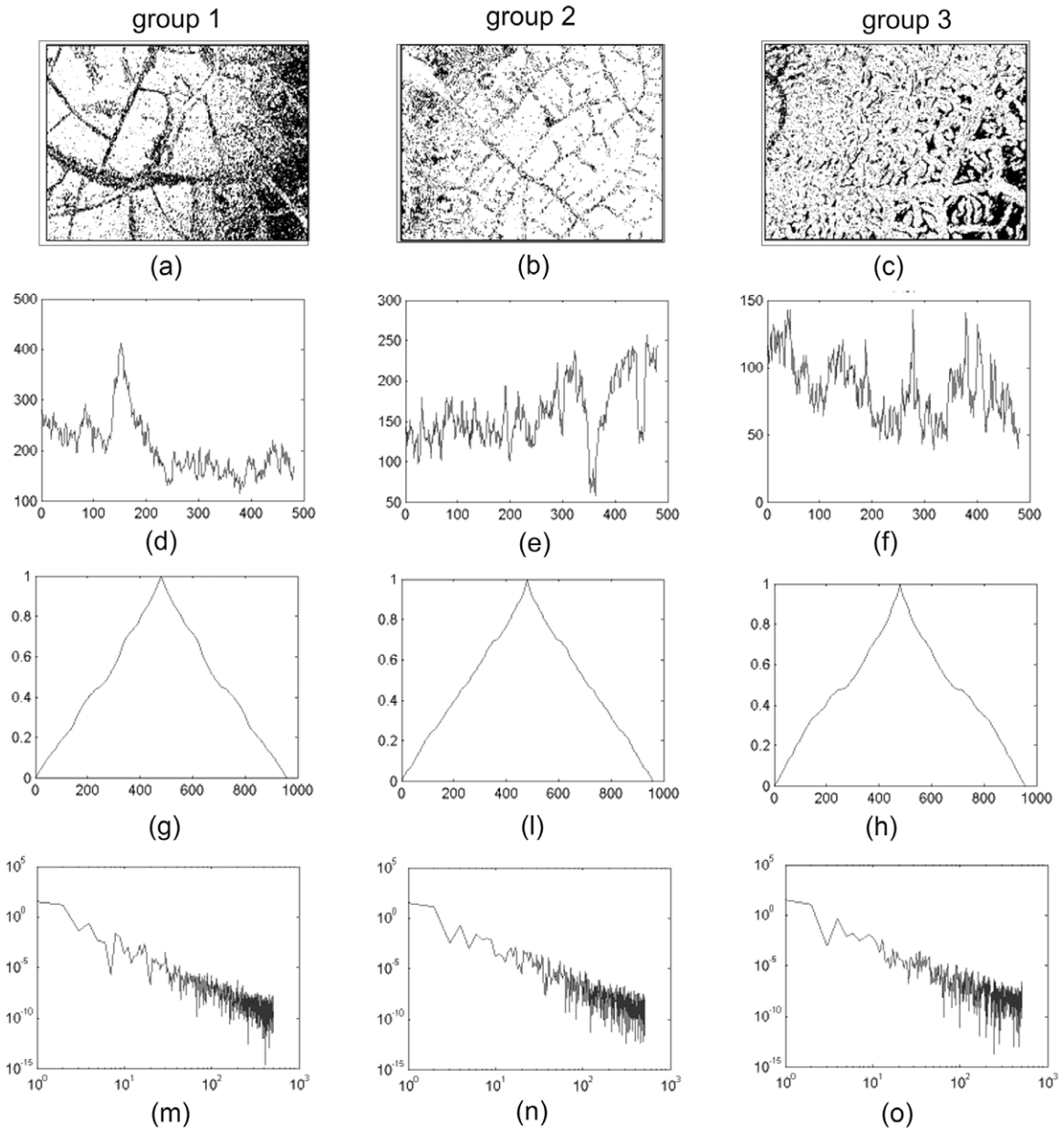

Figure 3. Coordinate $V_4(m \times n) = 0$ (a)–(c) and quantitative $N_L(x)$ distributions (d)–(f) of L-states in polarization; autocorrelation functions $K_L(\Delta m)$ (g, l, h) and relations $\log J_L - \log d^{-1}$ (m)–(o) for power spectra $J(N_L)$ of the distribution $N_L(x)$ for laser images of the blood plasma layers.

($K_{\pm C}(\Delta m)$) and logarithmic ($\log J_{\pm C} - \log d^{-1}$) distributions for polarization-singular $\pm C$-states in laser images of blood plasma layers.

Optical manifestations of the anisotropic layer of the polycrystalline network of blood plasma proteins are illustrated with the network of $\pm C$-points in the laser image (figures 4(a)–(c)). It is seen that the total number of circularly polarized points in the laser images of blood plasma smears from patients with pathological changes (figures 4(d)–(f)) increased sequentially.

All the statistical moments $Z^{\pm C}_{j=1;2;3;4}$ that characterize the distribution $N_{\pm C}(x)$ of the number of circularly polarized singular states differ from zero: $Z_1^{\pm C} = 0.19$, $Z_2^{\pm C} = 0.31$, $Z_3^{\pm C} = 0.44$, $Z_4^{\pm C} = 0.58$ (group 1); $Z_1^{\pm C} = 0.29$, $Z_2^{\pm C} = 0.23$, $Z_3^{\pm C} = 0.87$, $Z_4^{\pm C} = 0.95$ (group 2); and $Z_1^{\pm C} = 0.34$, $Z_2^{\pm C} = 0.17$, $Z_3^{\pm C} = 1.54$, $Z_4^{\pm C} = 2.15$ (group 3).

For the laser image of blood plasma smears from patients with mastopathy the correlation area $S^{\pm C}$ and correlation moment $Q^{\pm C}$ of the distribution $N_{\pm C}(x)$ compared with similar correlation parameters of $N_L(x)$ distributions (figure 3(e)) show changes in inverse proportion: $S^{\pm C}(\downarrow) = 0.17$ and $Q^{\pm C}(\uparrow) = 0.59$.

In contrast to random distributions of the number of $\pm C$-states of laser images of blood plasma from healthy patients, the dependences of $N_{\pm C}(x)$ are transformed into multifractal form for patients with mastopathy. Such a tendency is illustrated by the corresponding approximated

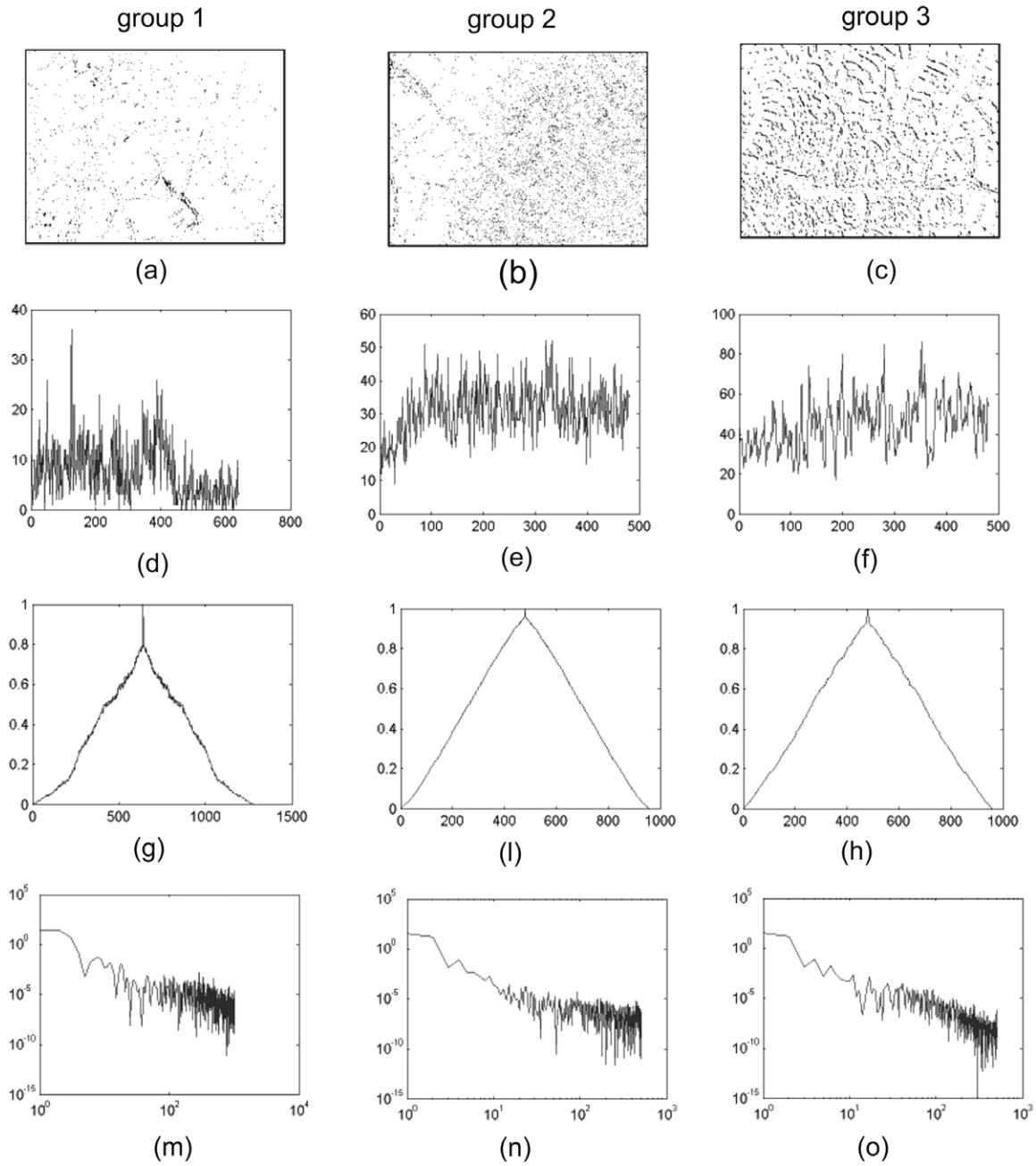

Figure 4. Coordinate $V_4(m \times n) = 1$ (a)–(c), and quantitative $N_{\pm C}(x)$ distributions (d)–(f), of $\pm C$-states in polarization autocorrelation functions $K_{\pm C}(\Delta m)$ (g, h) and dependences $\log J_L - \log d^{-1}$ (m)–(o) for power spectra $J(N_{\pm C})$ of the distribution $N_{\pm C}(x)$ for laser images of blood plasma layers for all groups.

lines to the logarithmic dependences $\log J_{\pm C} - \log d^{-1}$ (figures 4(m), (n)).

The total number of L- and $\pm C$-states of polarization for the respective laser images of blood plasma layers from patients with cancer is approximately the same (figures 3(f), 4(f)). As in the case of the $N_L(x)$ distribution for the number of linearly polarized states, the $N_{\pm C}(x)$ distribution is close to the equiprobable one: $Z^{\pm C}_{j=3;4} \prec\prec Z^{\pm C}_{j=1;2}$. Differences between statistical moments $Z^{L}_{j=1;2;3;4}$ and $Z^{\pm C}_{j=1;2;3;4}$ are insignificant and lie within 20–30%: $Z^{\pm C}_1 = 0.15$, $Z^{\pm C}_2 = 0.32$, $Z^{\pm C}_3 = 0.09$, $Z^{\pm C}_4 = 0.17$. The values of the correlation area $S^{\pm C}$ and correlation moment $Q^{\pm C}$ are close to their extremum ones: $S^{\pm C} = 0.23$; $Q^{\pm C} = 0.12$.

Our analysis of the logarithmic dependences (figure 4(o)) for the power spectra $J(N_{\pm C})$ of the $N_{\pm C}(x)$ distribution in laser images of the blood plasma layers for group 3 found a stable slope of the approximating curve: $F^{\pm C} = 2.11$. The statistically averaged (within the limits of groups 1–3) values and ranges of changing statistical moments $Z^{L;\pm C}_{j=1;2;3;4}$, correlation $Q^{L;\pm C}$, $S^{L;\pm C}$ and fractal $F^{L;\pm C}$, $D^{L;\pm C}$ parameters that characterize the $N_{\pm C}(x)$ dependences for the number of singular states in laser images of blood plasma layers are given in on table 1.

Table 1. Statistical, correlation and fractal parameters for the distribution of the number of polarization-singular states in laser images of blood plasma layers.

	Group 1		Group 2		Group 3	
$L-$; $\pm C-$	$L-$	$\pm C-$	$L-$	$\pm C-$	$L-$	$\pm C-$
Z_1	0.71 ± 0.079	—	0.43 ± 0.045	0.14 ± 0.032	0.25 ± 0.035	0.21 ± 0.041
Z_2	0.12 ± 0.034	—	0.23 ± 0.042	0.39 ± 0.091	0.32 ± 0.045	0.26 ± 0.034
Z_3	0.05 ± 0.008	—	0.07 ± 0.009	0.41 ± 0.12	0.05 ± 0.007	0.08 ± 0.01
Z_4	0.17 ± 0.044	—	0.08 ± 0.009	0.49 ± 0.23	0.08 ± 0.03	0.07 ± 0.05
S	0.27 ± 0.012	—	0.24 ± 0.02	0.18 ± 0.045	0.21 ± 0.032	0.26 ± 0.028
Q	0.08 ± 0.01	—	0.01 ± 0.0149	1.01 ± 0.35	0.18 ± 0.034	0.14 ± 0.019
F	2.01 ± 0.11	—	2.12 ± 0.012	—	2.23 ± 0.08	2.05 ± 0.11
D	0.25 ± 0.073	—	0.27 ± 0.012	0.49 ± 0.021	0.22 ± 0.019	0.25 ± 0.021

Table 2. The efficiency of singular analysis of blood plasma laser images in the diagnosis and differentiation of pathological breast states. (Note: $\otimes$, differentiation is impossible; $\oplus$, differentiation is possible.)

Blood plasma layers	Groups 1–2; 3		Groups 2–3	
Parameters	N_L	$N_{\pm C}$	N_L	$N_{\pm C}$
Z_1	$\oplus$	$\otimes$	$\otimes$	$\otimes$
Z_2	$\oplus$	$\otimes$	$\otimes$	$\otimes$
Z_3	$\otimes$	$\oplus$	$\otimes$	$\otimes$
Z_4	$\otimes$	$\oplus$	$\oplus$	$\oplus$
S	$\otimes$	$\otimes$	$\otimes$	$\otimes$
Q	$\otimes$	$\oplus$	$\oplus$	$\oplus$
F	$\otimes$	$\oplus$	$\otimes$	$\otimes$
D	$\otimes$	$\oplus$	$\otimes$	$\oplus$

The possibility of differentiating 'group' optical properties of all groups blood plasma layers is shown in table 2.

7. Conclusions

(1) This work analyzes the main physical mechanisms behind the formation of polarization singularities in laser images of blood plasma layers.

(2) Statistical, correlation and fractal parameters are given for polarization-singularity estimation of the optical properties inherent in blood plasma layers of all types.

(3) The ranges are determined for changing the set of criteria that characterize distributions of the number of polarization-singular states in laser images, which enabled us to realize diagnostic parameters for the differentiation of pathological breast changes.

References

[1] Prahl S A, Keijzer M, Jacques S L and Welch A J 1989 A Monte Carlo model of light propagation in tissue *SPIE Proc. Dosimetry of Laser Radiation in Medicine and Biology IS 5* pp 102–11

[2] Jacques S L and Wang L-H 1995 Monte Carlo modeling of light transport in tissues *Optical Thermal Response of Laser Irradiated Tissue* ed A J Welch and M J C van Gemert (New York: Plenum) pp 73–100

[3] Sterenborg H J C M, van Gemert M J C, Kamphorst W, Wolbers J G and Hogervorst W 1989 The spectral dependence of the optical properties of human brain *Lasers Surg. Med.* **4** 221–7

[4] Cheong W-F, Prahl S A and Welch A J 1990 A review of the optical properties of biological tissues *IEEE J. Quantum Electron.* **26** 2166–85

[5] Lara D and Dainty C 2005 Double-pass axially resolved confocal Mueller matrix imaging polarimetry *Opt. Lett.* **30** 2879–81

[6] Laude-Boulesteix B, De Martino A, Drevillon B and Schwartz L 2004 Mueller polarimetric imaging system with liquid crystals *Appl. Opt.* **43** 2824–32

[7] De Martino A, Kim Y-K, Garcia-Caurel E, Laude B and Drévillon B 2003 Optimized Mueller polarimeter with liquid crystals *Opt. Lett.* **28** 616–8

[8] Medeiros R C G, Soares J C and Sousa F B 2012 Natural enamel caries in polarized light microscopy: differences in histopathological features derived from a qualitative versus a quantitative approach to interpret enamel birefringence *J. Microsc.* **246** 177–89

[9] Shribak M and Oldenbourg R 2003 Techniques for fast and sensitive measurements of two-dimensional birefringence distributions *Appl. Opt.* **42** 3009–17

[10] Ushenko Yu A 2012 Concerted spatial-frequency and polarization-phase filtering of laser images of polycrystalline networks of blood plasma smears *J. Biomed. Opt.* **17** 117005

[11] Angelsky O V, Ushenko A G, Ushenko Yu A, Pishak V P and Peresunko A P 2009 Statistical, correlation and topological approaches in diagnostics of the structure and physiological state of birefringent biological tissues *Handbook of Photonics for Biomedical Science* ed V V Tuchin (London: Taylor and Francis) pp 21–67 doi:10.1201/9781439806296-c10

[12] Angelsky O V, Pishak V P, Ushenko A G and Ushenko Yu A 2007 Statistical and fractal structure of biological tissue Mueller matrix images *Optical Correlation Techniques and Applications* ed O Angelsky (Bellingham, WA: SPIE) pp 213–66 doi:10.1117/3.714999.ch4

[13] Ushenko Yu A 2005 Statistical structure of polarization-inhomogeneous images of biotissues with different morphological structures *Ukr. J. Phys. Opt.* **6** 63–70

[14] Ushenko A G, Burkovets D M, Yermolenko S B, Arkhelyuk A D, Ushenko Yu A, Pishak V P, Pishak O V, Grigorishin P M and Zimnyakov D A 1999 Polarized microstructure of laser radiation scattered by optically active biotissues *Proc. SPIE* **3904** 542–8

[15] Olar E I, Ushenko A G and Ushenko Yu A 2004 Polarization correlation measurements of the phase tomograms of optically anisotropic biofractals *Laser Phys.* **14** 1115–21

[16] Angelsky O V, Gorsky M P, Maksimyak P P, Maksimyak A P, Hanson S G and Zenkova C Yu 2011 Investigation of optical currents in coherent and partially coherent vector fields *Opt. Express* **19** 660–72
[17] Angelsky O V, Yermolenko S B, Zenkova C Yu and Angelskaya A O 2008 Polarization manifestations of correlation (intrinsic coherence) of optical fields *Appl. Opt.* **47** 5492–9
[18] Angelsky O V, Ushenko A G, Burkovets D N and Ushenko Yu A 2002 Laser polarization visualization and selection of biotissue images *Opt. Appl.* **32** 591–601
[19] Nye J F and Berry M 1974 Dislocations in wave trains *Proc. R. Soc. Lond.* A **336** 165–90
[20] Nye J F 1999 *Natural Focusing and Fine Structure of Light: Caustics and Wave Dislocations* (Bristol: Institute of Physics Publishing)
[21] Soskin M, Denisenko V and Egorov R 2004 Topological networks of paraxial ellipse speckle-fields *J. Opt. A: Pure Appl. Opt.* **6** S281–7
[22] Freund I, Soskin M S and Mokhun A I 2002 Elliptic critical points in paraxialoptical fields *Opt. Commun.* **207** 223–53
[23] Soskin M S, Denisenko V and Freund I 2003 Optical polarization singularities and elliptic stationary points *Opt. Lett.* **28** 1475–7
[24] Dennis M R 2002 Polarization singularities in paraxial vector fields: morphology and statistics *Opt. Commun.* **213** 201–21
[25] Berry M V and Hannay J H 1977 Umbilic points on Gaussian random surfaces *J. Phys. A: Math. Gen.* **10** 1809–21
[26] Soskin M S, Denisenko V G and Egorov R I 2006 Singular elliptic light fields: genesis of topology and morphology *Proc. SPIE* **6254** 625404
[27] Schoonover R W and Visser T D 2006 Polarization singularities of focused, radially polarized fields *Opt. Express* **14** 5733–45
[28] Nye J F 1983 Lines of circular polarization in electromagnetic wavefields *Proc. R. Soc. Lond.* A **389** 279–90
[29] Flossmann F, Schwarz U T, Maier M and Dennis M R 2005 Polarization singularities from unfolding an optical vortex through a birefringent crystal *Phys. Rev. Lett.* **95** 253901
[30] Flossmann F, Schwarz U T, Maier M and Dennis M R 2006 Stokes parameters in the unfolding of an optical vortex through a birefringent crystal *Opt. Express* **14** 11402–11
[31] Bliokh K Y, Niv A, Kleiner V and Hasman E 2008 Singular polarimetry: evolution of polarization singularities in electromagnetic waves propagating in a weakly anisotropic medium *Opt. Express* **16** 695–709
[32] Volyar A V, Zhilaitis V Z and Shvedov V G 1999 Optical eddies in small-mode fibers: 2. The spinorbit interaction *Opt. Spectrosc.* **86** 664–70
[33] Shvedov V, Izdebsskaya Ya, Alkseev A and Volyar V 2002 The formation of optical vortices in the course of light diffraction on a dielectric wedge *Tech. Phys. Lett.* **28** 256–9
[34] Fadeyeva T, Rubass A, Egorov Y, Volyar A and Swartzlander G Jr 2008 Quadrefringence of optical vortices in a uniaxial crystal *J. Opt. Soc. Am.* A **25** 1634–41
[35] Ushenko Yu A 2011 Wavelet analysis of polarization maps of polycrystalline biological fluids networks *Opto-electron. Rev.* **19** 425–34
[36] Ushenko Yu A, Ushenko V A, Dubolazov A V, Balanetskaya V O and Zabolotna N I 2012 Mueller-matrix diagnostics of optical properties of polycrystalline networks of human blood plasma *Opt. Spectrosc.* **112** 884–92
[37] Ushenko Yu A, Olar O I, Dubolazov A V, Balanetskaya V O, Unguryan V P, Zabolotna N I and Oleinichenko B P 2011 Mueller-matrix diagnostics of optical properties inherent to polycrystalline networks of human blood plasma *Semicond. Phys. Quantum Electron. Optoelectron.* **14** 98–105
[38] Ushenko Yu A 2011 Investigation of formation and interrelations of polarization singular structure and Mueller-matrix images of biological tissues and diagnostics of their cancer changes *J. Biomed. Opt.* **16** 066006
[39] Angelsky O V, Ushenko A G, Burkovets D N, Ushenko Yu A, Jozwicki R and Patorski K 2002 Automatic polarimetric system for early medical diagnosis by biotissue testing *Opt. Appl.* **32** 603–12